U.S. DEPARTMENT OF ENERGY

PNNL-20507

Prepared for the U.S. Department of Energy
under Contract DE-AC05-76RL01830

Pore-Water Extraction Intermediate-Scale Laboratory Experiments and Numerical Simulations

M Oostrom
VL Freedman
TW Wietsma
MJ Truex

June 2011

Pacific Northwest
NATIONAL LABORATORY

DISCLAIMER

PACIFIC NORTHWEST NATIONAL LABORATORY
operated by
BATTELLE
for the
UNITED STATES DEPARTMENT OF ENERGY
under Contract DE-AC05-76RL01830

Printed in the United States of America

Available to DOE and DOE contractors from the
Office of Scientific and Technical Information,
P.O. Box 62, Oak Ridge, TN 37831-0062;
ph: (865) 576-8401
fax: (865) 576-5728
email: reports@adonis.osti.gov

Available to the public from the National Technical Information Service,
U.S. Department of Commerce, 5285 Port Royal Rd., Springfield, VA 22161
ph: (800) 553-6847
fax: (703) 605-6900
email: orders@ntis.fedworld.gov
online ordering: http://www.ntis.gov/ordering.htm

This document was printed on recycled paper.
(9/2003)

PNNL-20507

Pore-Water Extraction Intermediate-Scale Laboratory Experiments and Numerical Simulations

M Oostrom
VL Freedman
TW Wietsma
MJ Truex

June 2011

Prepared for
the U.S. Department of Energy
under Contract DE-AC05-76RL01830

Pacific Northwest National Laboratory
Richland, Washington 99352

Summary

Pore-water extraction is considered as a method to remove water, containing contaminants such as technetium-99 (^{99}Tc), from the vadose zone at the Hanford Site. In the method, a negative pressure (suction) is applied at the extraction well, potentially forcing water to move to the well due to a resulting water pressure gradient. A pore-water extraction process should not be considered to be equal to soil vapor extraction because during soil vapor extraction, the main goal is to maximize gas removal. For pore-water extraction, however, the goal is to remove liquid water (and dissolved components) and care should be taken to create a hydraulic gradient towards the removal well for the range in capillary pressure (gas pressure minus water pressure) associated with a reasonable range in water contents. For pore-water extraction systems, pressure gradients in both the gas and water phases need to be considered while for soil vapor extraction purposes, gas phase flow is the only concern.

A series of six flow cell experiments was conducted to demonstrate the process of water removal through pore-water extraction in unsaturated systems. The intermediate-scale flow cell was especially designed and constructed for this purpose. The experimental configurations consist of homogeneous packings, which represent, in terms of particle size distribution, targeted subsurface sediments at the SX Tank Farm that contain high moisture contents and high contaminant concentrations. The porous media used in the actual experiments were mixtures of several classes of other Hanford sediments to arrive at the selected particle size distribution. The water in the flow cell experiments did not contain contaminants such as ^{99}Tc.

In the six experiments, the variables considered were the imposed negative pressure (100 cm and 200 cm), initial water content (0.11 and 0.18), water supply (no flow boundary condition and a condition where extracted water was replenished), and the inclusion of a fine-grained well-pack sand. The experiments without the well-pack sand were conducted for 7 days while the experiments with the well-pack sand lasted for 10 days. Water content as a function of time and water pressures at four locations were collected. For the experiments with the well-pack sand, gas pressures were also obtained at the same locations.

In the experiments where a zero flux water boundary condition was imposed, the results show that application of a negative pressure (vacuum) in a controlled manner leads to pore-water extraction until the water pressure gradients towards the extraction boundary approach zero. A few scoping tests indicated that when that boundary pressure was applied instantaneously, virtually no water outflow was obtained because of the likely formation of larger conduits from which air could easily be conducted. For field applications, it is recommended that the imposed vacuum be slowly increased to avoid the water continuity problems observed in the laboratory.

Another experimental observation was that after water extraction had ceased, continued application of the vacuum resulted in desiccation near the boundary where gas was entering the flow cell. In that case, the incoming air had a humidity of around 30% and water was removed from the porous medium as this air moved through the flow cell. Injection of air with a higher humidity would potentially lead to increases in water content due to condensation of water, potentially leading to vertical water movement, and is therefore not recommended.

Additional simple scoping experiments in l-m-long columns indicated that the relative permeability of uniform coarse- and medium-grained sands during pore-water extraction decreased rapidly to a point where virtually no water outflow was observed. To avoid that problem, a fine-grained well-pack sand was used instead with an entry pressure greater than the imposed vacuum of 100 cm. Inclusion of a fine-grained saturated well-pack sand resulted in lower production rates than the case without well-pack sand. Although limited, this set of experiments suggest that the design of the well and associated well-pack sands are critical to pore-water extraction performance.

Increased cumulative outflow was obtained with an increase in initial water content, applied negative pressure (suction), and when the water-supplying sediment was not limited. The experimental matrix was not sufficiently large to come to conclusions regarding maximizing cumulative outflow.

The experiments demonstrate that pore-water extraction from unsaturated porous media is, in principle, possible under the highly controlled conditions in the laboratory. The design was such that the moving air was forced to travel through sediment containing the pore water available for extraction. Under field conditions, water outflow rates may be negatively affected by preferential gas flow in relatively dry coarse-grained high permeability sediments. More complex systems with horizontal heterogeneities were not investigated in this study.

The outflow and pressure predictions were reasonably close to the experimental observations for all experiments. This result demonstrates that numerical simulations can be used with some level of confidence to support the design of field-scale applications of this method. Some of the reasons good agreement between numerical and experimental results were obtained include the independent determination of hydraulic properties and the control of the experimental boundary and initial conditions.

Acknowledgments

This work was funded by Washington River Protection Solutions.

Abbreviations and Acronyms

99Tc	technetium-99
°C	degree(s) Celsius
cm	centimeter(s)
cm3	cubic centimeter(s)
ft	foot(feet)
g	gram(s)
in.	inch(es)
kg	kilogram(s)
L	liter(s)
m2	square meter(s)
m3	cubic meter(s)
min	minute(s)
mL	milliliter(s)
Pa	Pascal(s)
pCi	picocurie(s)
s	second(s)

Contents

Figures

Tables

1.0 Introduction

Washington River Protection Solutions contracted with Pacific Northwest National Laboratory to conduct laboratory experiments to examine the process of extracting pore water from unsaturated sediment using an imposed vacuum. The tests specifically examined pore water extraction for sediment conditions relevant to the vadose zone beneath the SX Tank Farm at Hanford Site in southeastern Washington State. As part of previous test-site characterization for a field-scale treatability test of soil desiccation conducted at Hanford, soil gas was withdrawn from a 4-in.-diameter well over a 20-ft screened interval at a rate of about 400 cfm (DOE 2010). Nitrate and technetium-99 (^{99}Tc) concentrations measured in the water condensate from this soil gas extraction suggest that pore water was extracted from the sediment and entrained in the exhausted soil gas. Pore-water extraction offers the possibility of contaminant and water removal from the vadose zone and thereby may be beneficial in reducing the flux of vadose zone contaminants to the groundwater.

Previously, a limited set of numerical simulations examined the phenomena of pore-water extraction for selected sand, silt, and clay sediment properties and concluded that application of negative pressure to induce a pressure gradient across sediment could move pore water, with the most movement occurring in the silt sediment compared to the sand or clay sediment. Pore-water extraction cannot remove all of the pore water, just a portion of water above a threshold water content (part of the total volume occupied by water) that is a function of the sediment properties and imposed vacuum (negative pressure). The simulation results also suggest that the pore-water extraction process can potentially be sustained as long as water content conditions remain above the threshold for pore-water movement. Methods to replenish the removed water, such as high-humidity air injection, to aid in the removal additional ^{99}Tc, have to be used with caution. Unless the subsurface temperature is controlled, water condensation at locations with a lower temperature might occur, potentially leading to undesired vertical downward movement of the introduced water including contamination.

The above observations from the desiccation test site characterization and the previous numerical simulations suggest that application of a vacuum may lead to removal of pore water if conditions are such that sufficient pressure gradients are generated to drive water to the extraction wells. Soil vapor does not contain dissolved contaminants, which reside in the pore water. Therefore, the removal of pore water (and the dissolved contaminants) is of interest and was the subject of this research project.

A series of flow cell experiments was conducted to further investigate and demonstrate the process of water removal through pore-water extraction in unsaturated systems. In this process, a vacuum (negative pressure) is applied at the extraction well establishing a water pressure gradient towards the well. The gradient may force water and dissolved contaminants, such as ^{99}Tc, to move towards the well. The tested configurations consist of homogeneous packings, with or without fine-grained well-pack material, representing, in terms of particle size distribution, subsurface sediments at the SX Tank Farm. The water used in the experiments did not contain contaminants and no direct observations were made to study contaminant behavior under the tested flow conditions.

The ensuing sections of this report describe the materials and methods used and present results and conclusions of the flow cell experiments.

2.0 Materials and Methods

The laboratory experiments and associated numerical model for this research project are described below.

2.1 Laboratory Experiments

A porous medium was selected to represent the SX Tank Farm subsurface, the hydraulic properties of the sediment were determined, and a series of six flow cell experiments was designed and conducted.

2.1.1 Porous Medium Selection for SX Tank Farm Subsurface Representation

A requirement of the porous medium to be used in the experiments was that it had to represent the subsurface below the SX tanks where a combination of high moisture contents and contaminant concentrations would exist. Characterization data from Serne et al. (2002a; borehole 299-W23-19), Serne et al. (2002b; borehole 299-W23-234), and Serne et al. (2002c; 241-SX-108 slant borehore) were compiled to determine a representative particle size distribution that could be reconstructed with available Hanford sediments in the laboratory.

Water contents and ^{99}Tc concentrations for borehole 299-W23-19 are shown in Figure 2.1 along with the hydrogeologic unit designations used in this report (e.g., H2, PPlz). The plots show higher moisture contents in the H2 unit (~10%), with ^{99}Tc concentration less than 1,000 pCi/mL, and in the PPlz unit (~15%) with a maximum ^{99}Tc concentration around 3,200 pCi/mL at 130 ft. Representative particle size distributions for the H2 unit are 0% gravel, 93% sand, and 7% silt/clay. For the PPlz unit at 130 ft, there is no gravel, only 17% sand, and 83% silt/clay. At borehole 299-W23-234 (Figure 2.2), higher moisture contents are again found in the H2 unit (~11%), with ^{99}Tc concentration up to $1.2\ 10^4$ pCi/mL at 108.5 ft, but low concentrations in the PPlz unit with a maximum ^{99}Tc concentration <330 pCi/mL. Representative particle size distributions for the H2 unit at 108.5 ft are 0.05% gravel, 65.47% sand, and 31.62% silt/clay. The slant borehole (Figure 2.3) shows moisture contents of about 7% in the H2 unit and 11% in the PPlz unit. The maximum concentration is ~$2.5\ 10^5$ pCi/mL at 98 ft in the H2 unit and ~$1.0\ 10^5$ pCi/mL at 130 ft in the PPlz unit. The particle size distribution for the H2 unit in this borehole is 0.29% gravel, 63.6% sand, and 39% silt/clay. For the PPlz unit at 130 ft, there is 59.6% silt/clay and 40.4% sand. Based on this information, it was decided to use a particle size distribution of 0.0% gravel, 65% sand, and 35% silt/clay. The selected particle size distribution was then created by mixing the following components:

- <53 mm: 35 % (silt/clay fraction)
- 53 mm – 0.250 mm: 40%
- 0.250 mm – 0.5 mm: 20%
- 0.5 mm – 1 mm: 4%
- 1 mm – 2 mm: 1%.

Because the mixture is not sediment directly obtained from the SX Tank Farm but constructed from other Hanford sediments, it will be referred to in this report as SXsim (SX simulant) sediment.

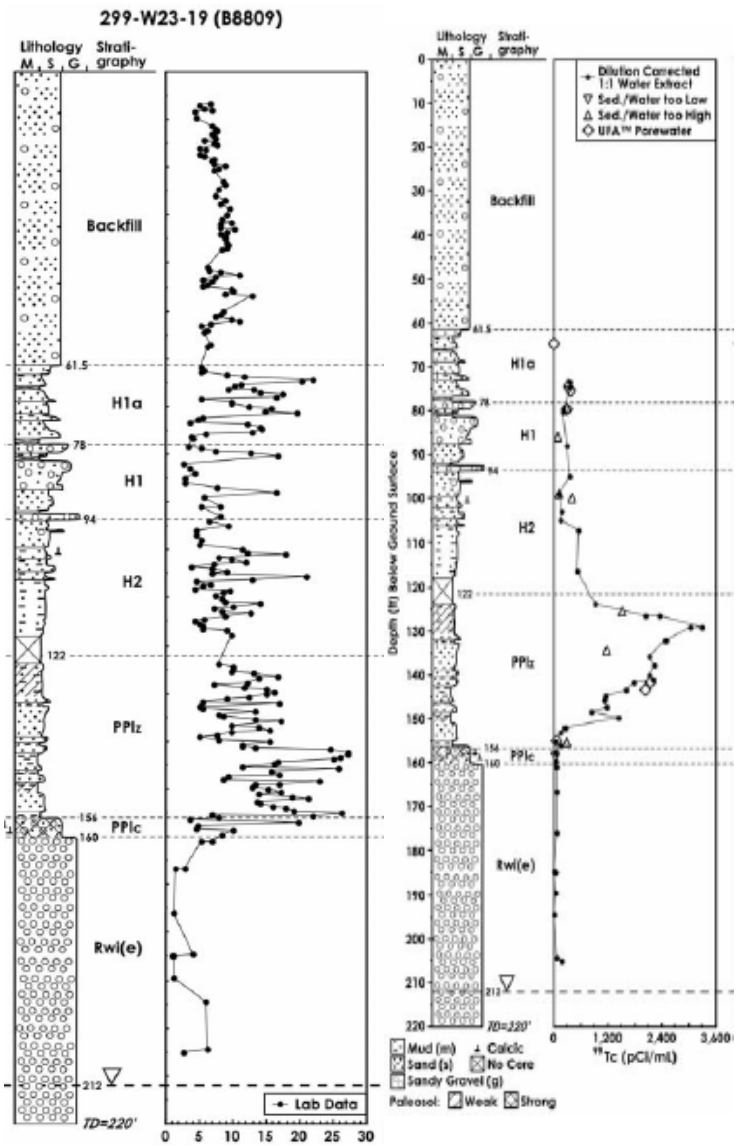

Figure 2.1. Moisture Content and ^{99}Tc Distribution for Borehole 299-W23-19 (after Serne et al. 2002a)

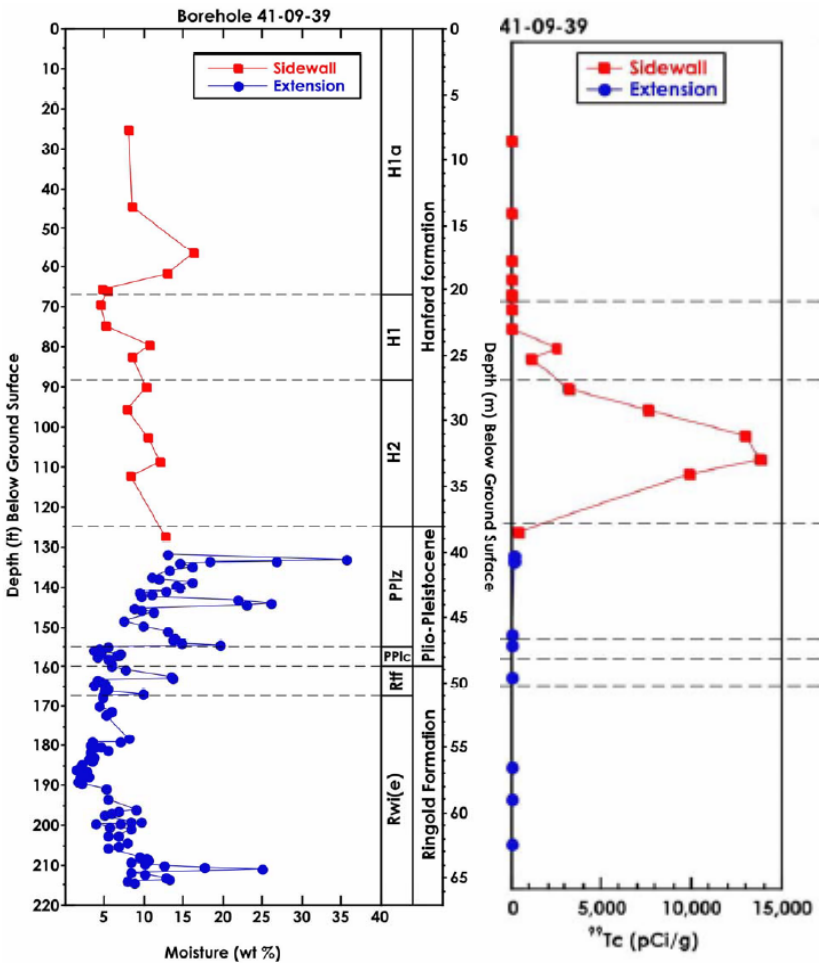

Composite Depth (ft bgs)[a]	1:1 Extract ID	^{99}Tc (pCi/L)
90	06A/B	2.7E+06
	6 UFA	2.48E+07
95.5	03A/B/C	7.1E+06
102.5	05A/B/C	6.1E+06
108.5	04A/B/C	1.2E+07
	4 UFA	9.40E+07
112	02B/C	8.6E+06
	2 UFA	1.23E+08
127.4	01A/B/C	3.3E+05

Figure 2.2. Moisture Content and ^{99}Tc Distribution for Borehole 299-W23-234 (after Serne et al. 2002b)

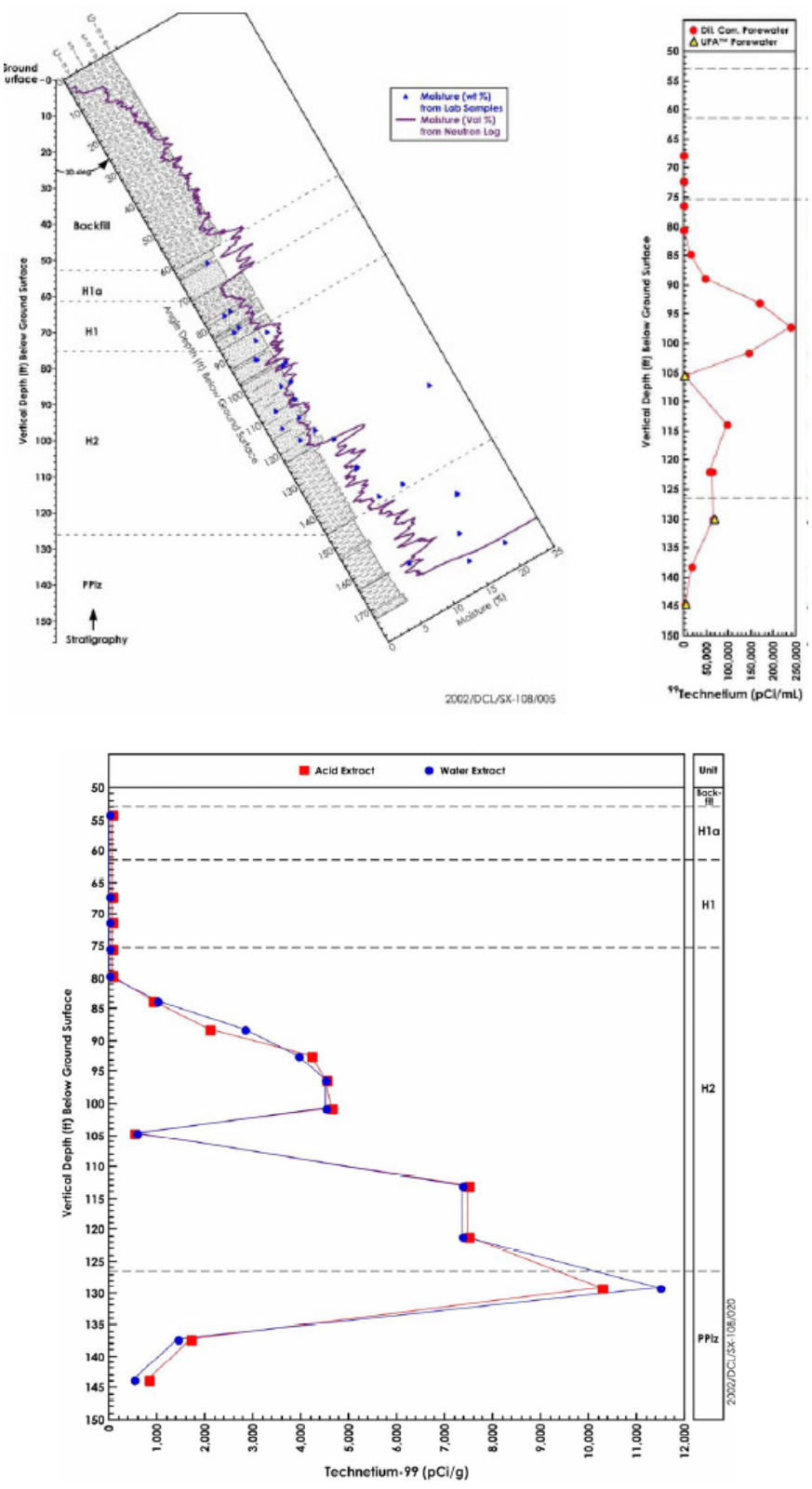

Figure 2.3. Moisture Content and ^{99}Tc Distribution for the 241-SX-108 Slant Borehole (after Serne et al. 2002c)

2.1.2 Sediment Hydraulic Properties

Hydraulic properties of both the SXsim and a well-pack sand (140-mesh sand) were obtained using procedures described by Schroth et al. (1996) and Wietsma et al. (2009). The obtained values are listed in Table 2.1. The hydraulic properties experimental setup is shown in Figure 2.4. For each material, permeability (L^2) was obtained first using the constant head method (Wietsma et al. 2009) for cores with a length of 15 cm and an internal diameter of 9.525 cm. The cores were packed with damp porous media (25 g water per kilogram of sediment) in lifts of one cm. After packing each layer, the surface was gently scratched before the next layer was emplaced. This method prevents distinct layering of the porous media and was also used to pack the intermediate-scale flow cells. The porosity was obtained using a particle density of 2.70 g/cm^3. After packing, the samples were slowly saturated until a saturated equilibrium condition was obtained as indicated by pressure readings from two transducers, located at 2.5 and 12.5 cm from the bottom of the cores. Permeability values were obtained in triplicate using heads of 7.5 and 15 cm. The average value is listed in Table 2.1. After the permeability measurements, a sintered metal plate with an entry pressure of 200 cm was attached to the bottom of the core and the core was subsequently drained by applying increased air pressure at the top. Water pressures and displaced water were recorded as a function of time. The data were then fitted to the van Genuchten (1980) retention relation using a procedure described by Schroth et al. (1996). The van Genuchten (1980) relation is given by

$$\theta = \theta_r + (\theta_s - \theta_r)\left(\frac{1}{1+(\alpha h)^n}\right)^m \tag{2.1}$$

where θ = actual moisture content

θ_s = saturated moisture content

θ_r = irreducible moisture content (water volume divided by the total volume

h = water pressure head (cm),

α and n = pore-shape factors, and $m = 1 - 1/n$.

The fitted lines for both porous media are shown in Figure 2.5. The relation for the 140-mesh sand indicates its relatively high entry pressure (>100 cm), which is the pressure where the largest pores of the sediment start to release water. The relation for the 140-mesh also indicates a narrow pore size distribution, leading to rapid drainage once the entry pressure has been exceeded. The SXsim material releases water at considerably lower pressures and water contents approach irreducible values at capillary pressures (gas pressure minus water pressure) close to 50 cm. In terms of the removal of pore water from porous media, it should be noted that water movement is determined by a gradient in the hydraulic pressure, while the associated water contents are a function of capillary pressure.

Table 2.1. Hydraulic Properties of SXsim Sediment and 140-Mesh Well-Pack Sand

Property	SXsim	140-Mesh Sand
Permeability (m^2)	1.23×10^{-12}	8.62×10^{-14}
Van Genuchten α (1/cm)	0.016	0.007
Van Genuchten n	3.24	7.8
Entry Pressure (cm)	21	114
Porosity	0.34	0.43
Irreducible Saturation	0.16	0.19

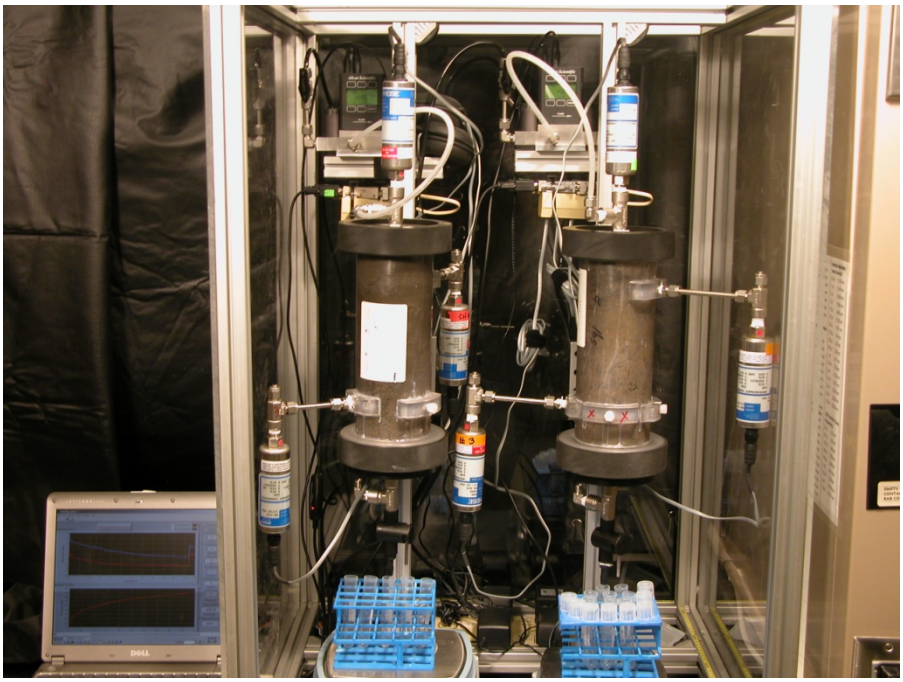

Figure 2.4. Hydraulic Properties Experimental Apparatus

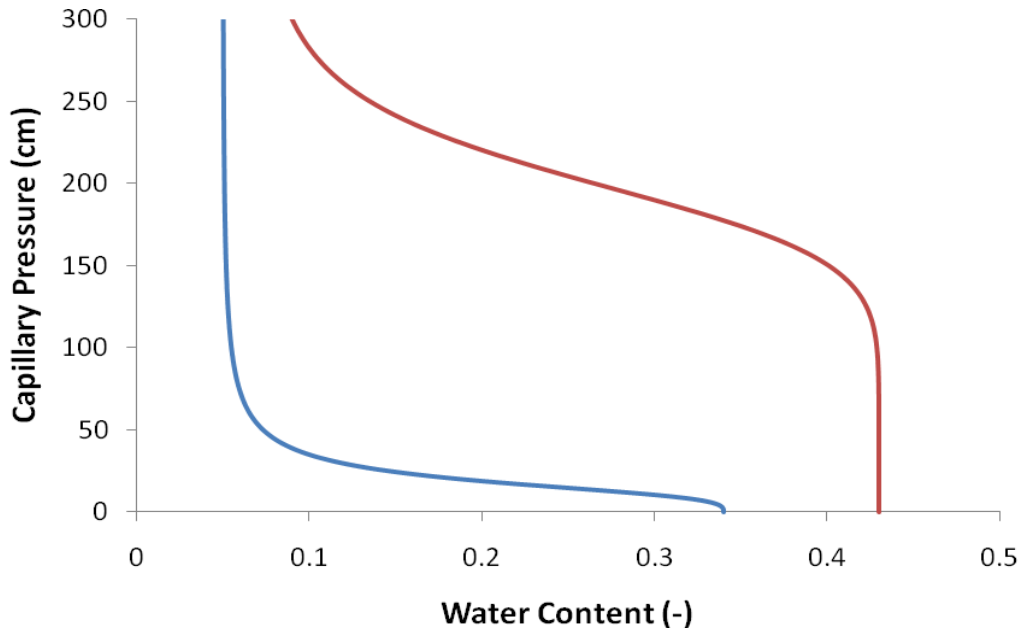

Figure 2.5. Fitted Capillary Pressure – Water Content Relations for SXsim (blue line) and 140-Mesh Sand (red line). Retention parameter values for both porous media are listed in Table 2.1. Capillary pressure is defined as the difference between gas and water pressure. Water content is defined as the volume of water divided by the total volume of the core.

2.1.3 Experimental Design

Six experiments were conducted in a flow cell with internal dimensions of 100 cm (length), by 20 cm (height), and 5 cm (width). It should be noted that the water used in the experiments did not contain ^{99}Tc or any other contaminants. An overview of the six experiments is provided in Table 2.2. Schematics of the experiments without well-pack sand (Exp. 1 – 4) and with the well-pack sand (Exp. 5 – 6) are provided in Figure 2.6 and Figure 2.7, respectively. The lower-left hand corner of the flow cell is denoted as (x = 0 cm, z = 0 cm). The volume of the flow cell, fabricated out of 3/8–in. polycarbonate, is 10 L. Water pressures were measured with stainless steel tensiometers, attached to Heise Model DXD pre-calibrated pressure transducers (Ashcroft Inc., Stanford, CT) at four locations: (x = 12.5 cm, z = 10 cm), (x = 37.5 cm, z = 10 cm), (x = 62.5 cm, z = 10 cm), and (x = 87.5 cm, z = 10 cm). Air was allowed to enter through four ¼-in. ports located at (x = 100 cm, z = 2.5 cm), (x = 100 cm, z = 7.5 cm), (x = 100 cm, z = 12.5 cm), and (x = 100 cm, z = 17.5 cm). Water and air were extracted from four ¼-in. ports located at (x = 0 cm, z = 2.5 cm), (x = 0 cm, z = 7.5 cm), (x = 0 cm, z = 12.5 cm), and (x = 0 cm, z = 17.5 cm). A picture of the flow cell used for Exp. 1 – 4 is shown in Figure 2.8. A detailed photograph of a Heiss pressure transducer and its connection to the flow cell is shown in Figure 2.9. The same transducer type was used to also measure gas pressures at the same locations for Experiments 5 and 6. A picture of the flow cell for the experiments with the well-pack sand (Exp. 5 – 6) is shown in Figure 2.10.

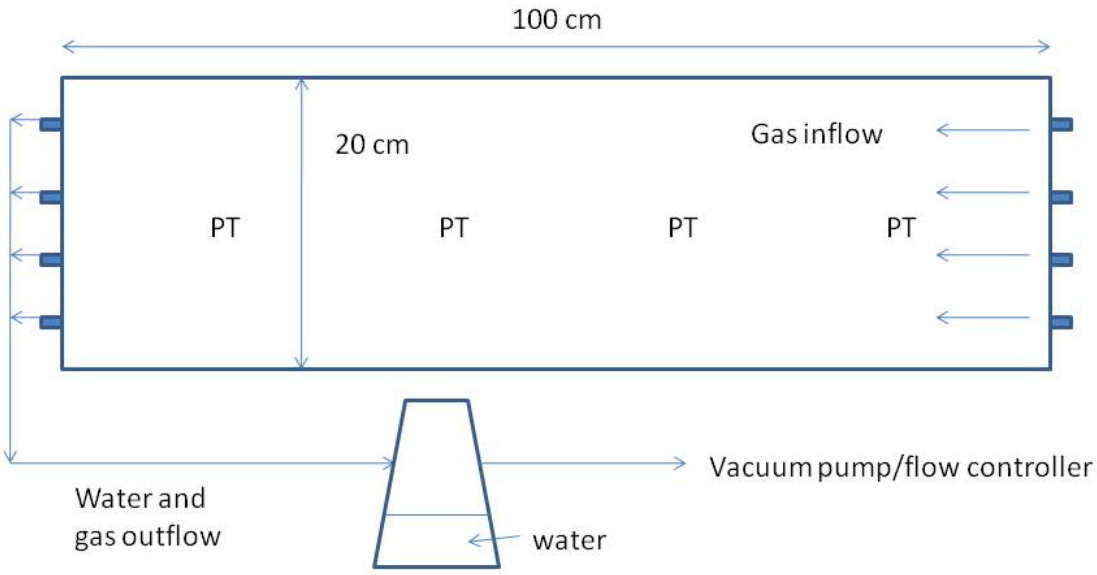

Figure 2.6. Schematic of the Experiments without the Well-Pack Sand (Experiments 1 – 4)

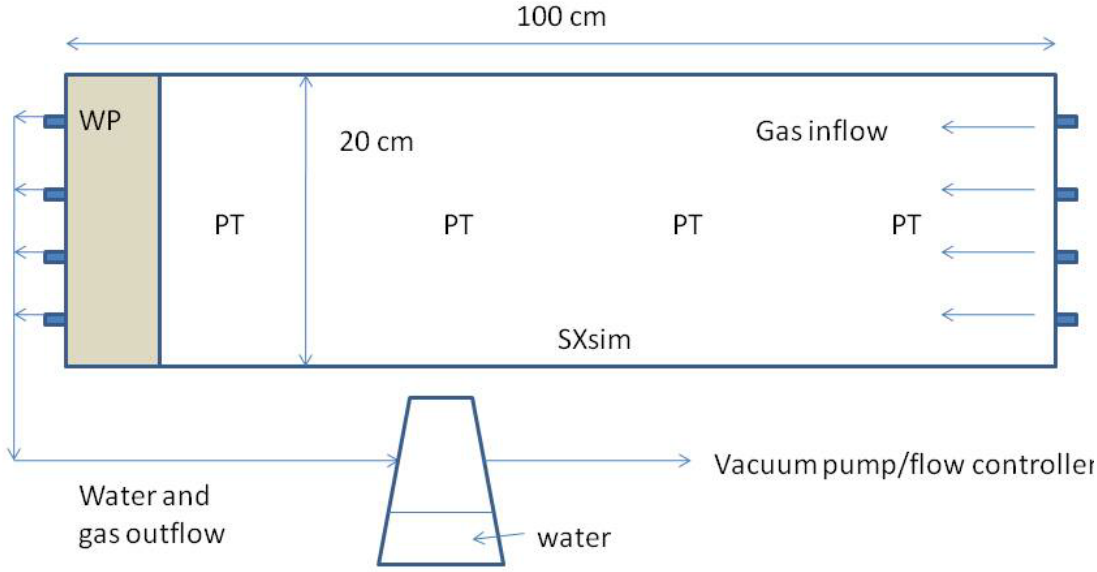

Figure 2.7. Schematic of the Experiments with the Well-Pack Sand (Experiments 5 and 6)

The flow cell was packed with the porous media under unsaturated conditions. The porous media were first mixed with 25 g/kg water before they were emplaced in 1-cm layers. After packing, the gas phase in the flow cell was replaced with CO_2 before water was injected at the lowest right-hand port (see Figure 2.6 and Figure 2.7) at a rate of 1 mL/min. Injection was stopped when the water level was at the top of the flow cell (z = 20 cm). The total water content in the SXsim material was ~0.34 in all experiments. Before vacuum was imposed, the flow cell was first drained until the initial moisture contents was achieved (0.11 for Experiments 1, 2, 4, 5, and 6; 0.18 for Experiment 3). The drainage process consisted of two phases. In the first phase, a water outlet was used at (x = 50 cm, z = 0 cm) to allow for free drainage. After the outflow stopped, a suction of 20 cm was temporarily imposed at the same location while keeping all boundaries closed. After a total removal of (0.34 – 0.11)/0.34 x 3400 = ~

2300 mL over both phases for Experiments 1, 2, 4, 5, and 6, and (0.34 – 0.18)/0.34 x 3400 = ~ 1600 mL for Experiment 3, water removal was stopped and the sediments were allowed to come to equilibrium for 2 days.

Table 2.2. Overview of Porous Media, Imposed Vacuum, Initial Moisture Content, and Upgradient Boundary Conditions for the Six Experiments

Experiment	Porous Media[(a)]	Imposed Vacuum (cm)[(b)]	Initial Moisture Content[(c)]	Upgradient Boundary Condition[(d)]
1	SXsim	100	0.11	No flow
2	SXsim	200	0.11	No flow
3	SXsim	100	0.18	No flow
4	SXsim	100	0.11	Flow out = Flow in
5	SXsim + WP	100	0.11	No flow
6	SXsim + WP	200	0.11	No flow

a. SXsim = porous medium prepared to mimic particle size distribution measured in W23-19 samples; SXsim + WP = well-pack porous medium added at discharge end of flow cell to mimic water movement to a well.
b. Delta pressure (base and one variant) selected based on discussion with WRPS for relevance to the field test.
c. Moisture content (base and one variant) based on data from W23-19 and boreholes near SX-108 and SX-109.
d. Experiments 1, 2, 3, 5, and 6 represent limited-size extraction zones. Experiment 4 simulates a laterally extensive extraction zone.

The pore-water extraction component was started by imposing a vacuum (negative pressure; Table 2.2) using an Allicat Scientific (Tucson, AZ) vacuum controller connected to the laboratory vacuum source. The pressure was decreased at a rate of 50 cm/min. The more gradual pressure decrease was needed because two initial scoping experiments using an instantaneous step change in pressure resulted in limited water outflow after an initial rapid production of a few grams of water. These observations may be attributed to rapid water drainage near the outlets and the formation of a high permeability conduit for gas as a result of the imposed rapid pressure change. The water relative permeability near the outlet might have been reduced to a level where no meaningful water flow out of the flow cell was possible. In Experiment 4, water was injected back into the flow cell at $x = 100$ cm with a rate equal to what was produced at $x = 0$ cm in the previous minute using a high-precision (< 0.5% coefficient of variance) Encynova Model 2-4 metering pump (Car-May LLC, Greeley, CO). The produced water mass was recorded as a function of time. The software to control the various steps in the experimental procedure was written in LabVIEW (National Instruments Corp., Austin, TX).

In Experiments 5 and 6, a 7.5 cm zone of 140-mesh sand was emplaced in the flow cell to mimic the behavior of a fine-grained well pack material. This particular sand fraction was obtained by sieving a 100-mesh Colorado Sand (Carmeuse Industrial Sands, Colorado Spring, CO) which contains approximately 20% of this fraction. A picture of this configuration is shown in Figure 2.10.

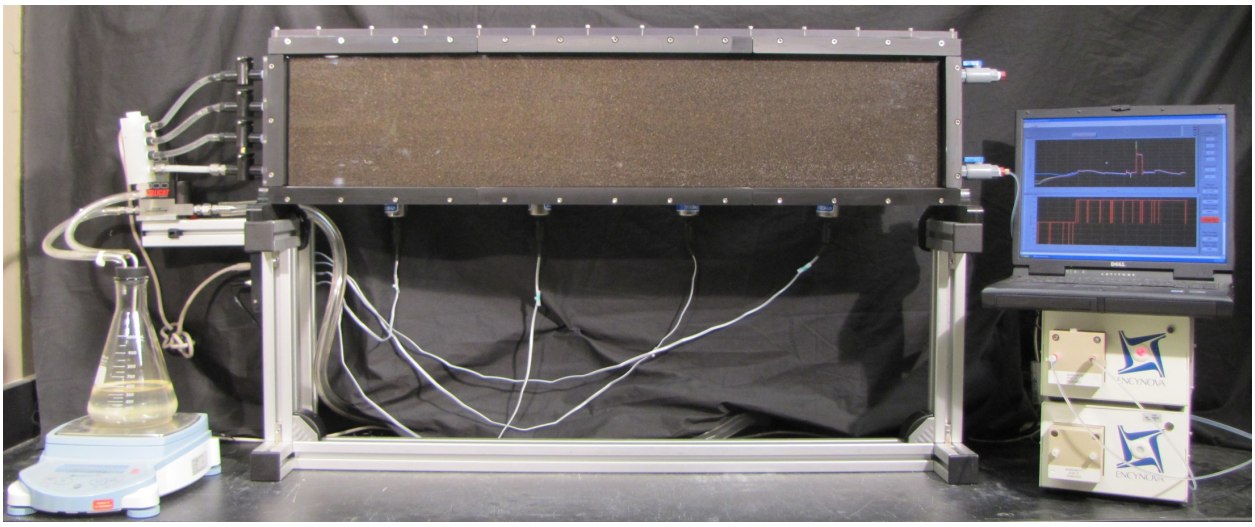

Figure 2.8. Flow Cell Experimental System for Experiments 1 – 4. The vacuum system is on the left. The pumps and data acquisition computer are on the right. The four water pressure transducers are located in the back of the flow cell.

Figure 2.9. Detailed View of Heiss Water Pressure Transducer Connected to the Flow Cell

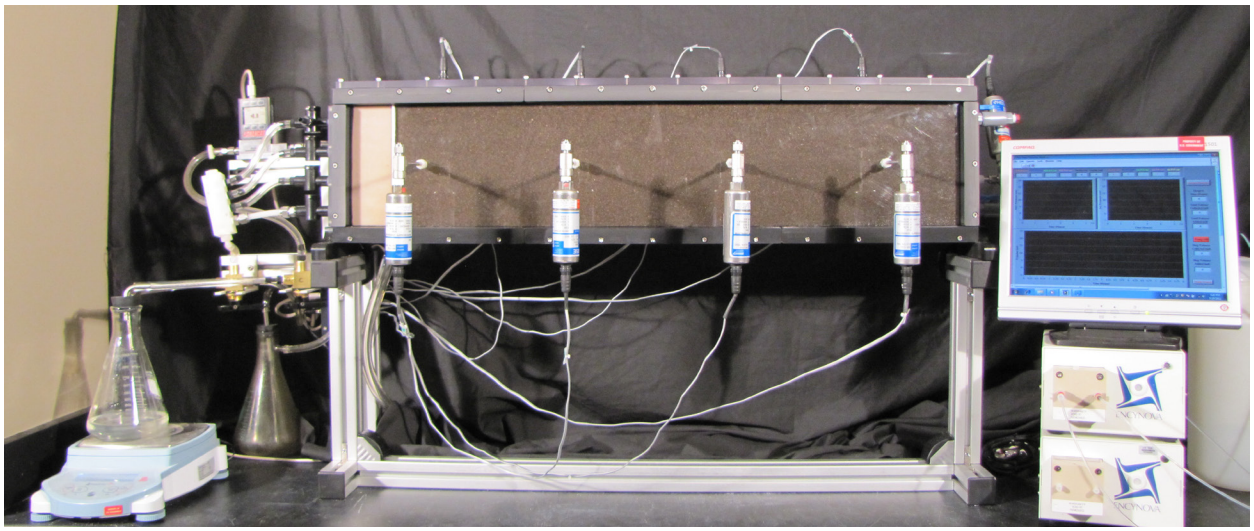

Figure 2.10. Flow Cell Experimental System for Experiments 5 – 6 with the 7.5 cm-wide, 140-Mesh, WellPack Sand. The vacuum system is on the left. The pumps and data acquisition computer are on the right. The four water pressure transducers are located in the front and the four air pressure transducers are located in the back.

2.2 Numerical Model

The simulations are conducted with the water-air-energy mode of the STOMP simulator (White and Oostrom 2006). The fully implicit integrated finite difference mode of the simulator has been used to simulate a variety of water-air systems (e.g., Oostrom et al. 2009). For the experiments listed in Table 2.2, constant temperature boundary conditions (20°C) are assumed, making solving the energy equation irrelevant. The applicable governing equations are the component mass-conservation equations for water and air:

$$\frac{\partial}{\partial t}\left[n_D \omega_l^w \rho_l s_l\right] = -\nabla F_l^w + \dot{m}^w \tag{2.1}$$

$$\frac{\partial}{\partial t}\left[\sum_{\gamma=l,g}\left(n_D \omega_\gamma^a \rho_\gamma s_\gamma\right)\right] = -\sum_{\gamma=l,g}\left\{\nabla F_\gamma^a + \nabla J_\gamma^a\right\} + \dot{m}^a \tag{2.2}$$

where

$$F_\gamma^w = -\frac{\omega_\gamma^w \rho_\gamma k_{rl} k}{\mu_\gamma}\left(\nabla P_\gamma + \rho_\gamma g z\right) \text{ for } \gamma = \text{l,g,} \tag{2-3}$$

$$F_\gamma^a = -\frac{\omega_\gamma^a \rho_\gamma k_{r\gamma} k}{\mu_\gamma}\left(\nabla P_\gamma + \rho_\gamma g z\right) \text{ for } \gamma = \text{l,g} \tag{2.4}$$

$$J_\gamma^a = -\tau_\gamma n_D \rho_\gamma s_\gamma \frac{M^a}{M_\gamma} D_\gamma^a \nabla \chi_\gamma^a \text{ for } \gamma = \text{l,g} \quad (2.5)$$

The subscripts l, and g denote aqueous and gas phases, respectively; the superscripts w and a denote water and air components, respectively; t is time (s), n_D is the diffusive porosity, n_T is the total porosity, ω is the component mass fraction, ρ is the density (kg/m^3), s is the actual liquid saturation, V is the volumetric flux (m/s), J is the diffusive-dispersive mass flux vector (kg/m^{2}s), m is the component mass source rate (kg/m^{3}s), k is the intrinsic permeability (m^2), $k_{r\gamma}$ is the relative permeability of phase γ, μ is the viscosity (Pa s), P is the pressure (Pa), g_z is the gravitational vector (m/s^2), τ is the tortuosity, M is the molecular weight (kg/mole), D is the diffusive-dispersive tensor (m^2/s), and χ is the component mole fraction. The governing partial differential equations (Equations 2.1a and 2.1b) are discretized following the integrated-volume finite difference method by integrating over a control volume. Using Euler backward time differencing, yielding a fully implicit scheme, a series of nonlinear algebraic expressions is derived. The algebraic forms of the nonlinear governing equations are solved with a multi-variable, residual-based Newton-Raphson iterative technique, where the Jacobian coefficient matrix is composed of the partial derivatives of the governing equations with respect to the primary variables.

Assuming the aqueous phase never disappears, the primary variable for the water equation is always the aqueous pressure. For the air equation, the primary variable is P_a. The algebraic expressions are evaluated using upwind interfacial averaging to fluid density, mass fractions, and relative permeability. Specified weights (i.e., arithmetic, harmonic, geometric, upwind) are applied to the remaining terms of the flux equations. For the simulations described in this report, harmonic averages were used and the maximum number of Newton-Raphson iterations was eight, with a convergence factor of 10^{-6}.

Secondary variables, those parameters not directly computed from the solution of the governing equations, are computed from the primary variable set through the constitutive relations. In this section, only the relations between relative permeability, fluid saturation, and capillary pressure (*k-S-P*) pertinent to the conducted simulations are described. The *k-S-P* relations consist of the van Genuchten (1980) *S-P* relations in combination with the *k-S* relations derived from the Mualem (1976) model. The *k-S-P* relations distinguish between actual and effective saturations. Actual saturations are defined as the ratio of fluid volume to diffusive pore volume. Effective saturations represent normalized actual saturations based on the pore volumes above the irreducible or minimum saturation of the wetting fluid (i.e., aqueous phase liquid).

The computation domain was discretized into uniform grid cells that are 1 cm in the x-direction, 5 cm in the y-direction, and 1 cm in the z-direction for a total number of nodes of 100 x 1 x 20 = 2000. Initially, water pressures were imposed over the domain so that the average saturation of the SXsim material was 0.11/0.34 = 0.323 for Experiments 1, 2, 4, 5, and 6. For the simulations of Experiment 3, the initial average saturation was 0.18/0.34 = 0.529. The pore-water extraction from these initial conditions was initiated by imposing a negative gas phase pressure at x = 0 cm. The water pressures at this boundary were allowed to follow the gas pressure by setting a Dirichlet-Outflow condition. This boundary condition ensures that the water pressure can never by higher than the gas pressure and that no water is allowed to move into the domain. At x = 100 cm, gas was allowed to move into the domain by specifying a constant atmospheric pressure. A zero flux boundary condition was used for the aqueous phase for Experiments 1, 2, 3, 5, and 6. For Experiment 4, the water that moved across the west boundary for each 1-minute time interval was injected over the next minute at the east boundary. Details of the numerical simulations can be found in the input file for Experiment 1, as listed in Appendix A.

3.0 Results

Results for the experimental matrix are presented in the next two sections.

3.1 Extraction from Experiments without Well-Pack Sand

Simulated and experimental cumulative outflow from the four homogeneous experiments (without well-pack sand) are shown in Figure 3.1. For all cases except Experiment 4, where water is injected at the right-hand side of the flow cell, the outflow rate is the highest almost immediately after imposing the boundary suction, and it slowly decreases over time. Due to the limited water availability in Experiments 1 – 3, the extraction rate decreases to nearly zero within a few days. For Experiment 4, the rate becomes a constant as near-equilibrium conditions are established in the flow cell. Experiment 4 was designed to show the effect of sustained production for an extended layer hydraulically connected to the extraction boundary. If extraction rates are able to be sustained in the field, the associated cumulative ^{99}Tc removal is also likely to increase with time.

The relative positions of the various results are consistent with expectations. An increased suction (Experiment 2) or a higher initial water content (Experiment 3) lead to increased cumulative outflow. In Experiment 4, the cumulative outflow is higher because no net desaturation takes place of the flow cell, as is shown by the near linearity of the outflow response curve. The simulated results agree reasonably well with the experiments and no major discrepancies are evident. The observed differences between model and experimental results are expected to be limited because the porous medium has been properly characterized and the boundary and initial conditions were controlled.

The observed water pressure response to the applied vacuum is relatively fast as is shown in Figure 3.2 – Figure 3.5 for Experiments 1 – 4, respectively. The observed responses are a function of distance to the extraction boundary but over time the water pressures asymptotically reach a value close to the imposed vacuum. The fact that the pressure values are getting closer as time progresses is consistent with the decreasing flow rate observations. Over time the pressure gradient decreases and a strongly reduced outflow rate is expected due to decreasing flow rates in the porous medium. For Experiment 4, where the inflow of water kept track of the extraction, the pressure gradients are more gradual over the length of the flow cell indicating sustained movement of water towards the outflow boundary.

After most of the mobile water was extracted from Experiment 1, sustained application of the 100-cm suction at the boundary was applied to observe its long-term effects. In this case, the application resulted in desiccation of part the flow cell because relatively large amounts of low-humidity gas were transported through the flow cell and dried out the right-hand side of the flow cell (Figure 3.4). Due to the limited supply of water left in the flow cell after the majority of the pore-extraction had taken place, the incoming air, with a humidity near 30%, started to remove the residual water in the form of water vapor. These conditions are not likely to develop in the field unless relatively dry air is injected into the subsurface.

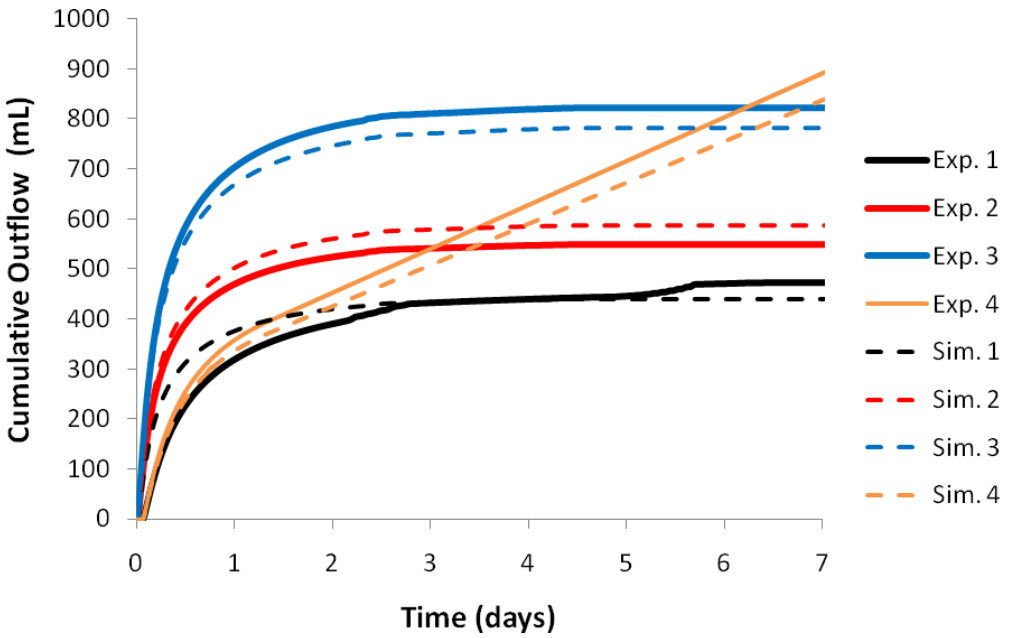

Figure 3.1. Simulated and Observed Cumulative Outflow (mL) as a Function of Time for Experiments 1 – 4

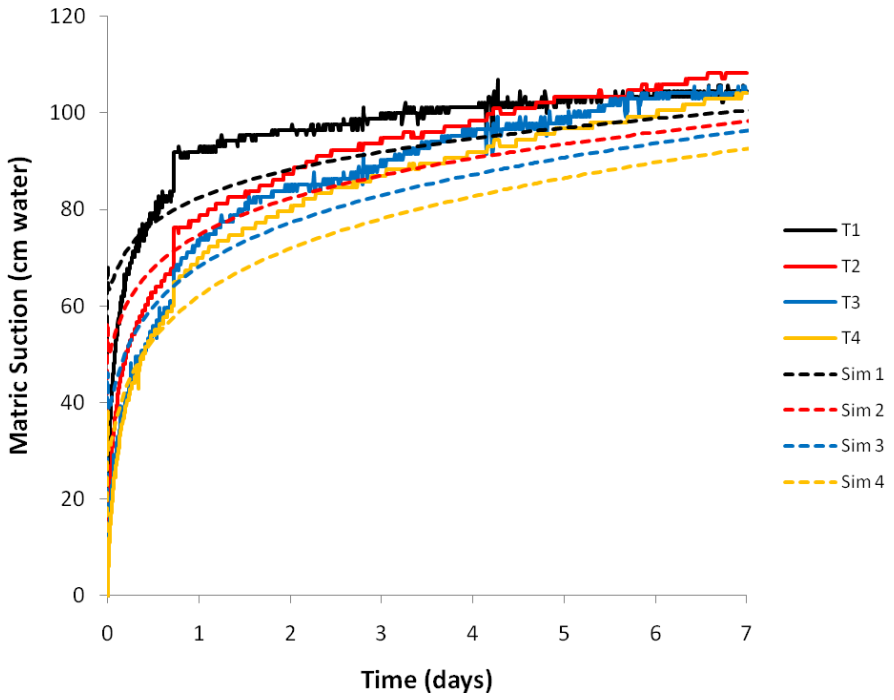

Figure 3.2. Measured and Simulated Matric Suctions (cm water) for Experiment 1

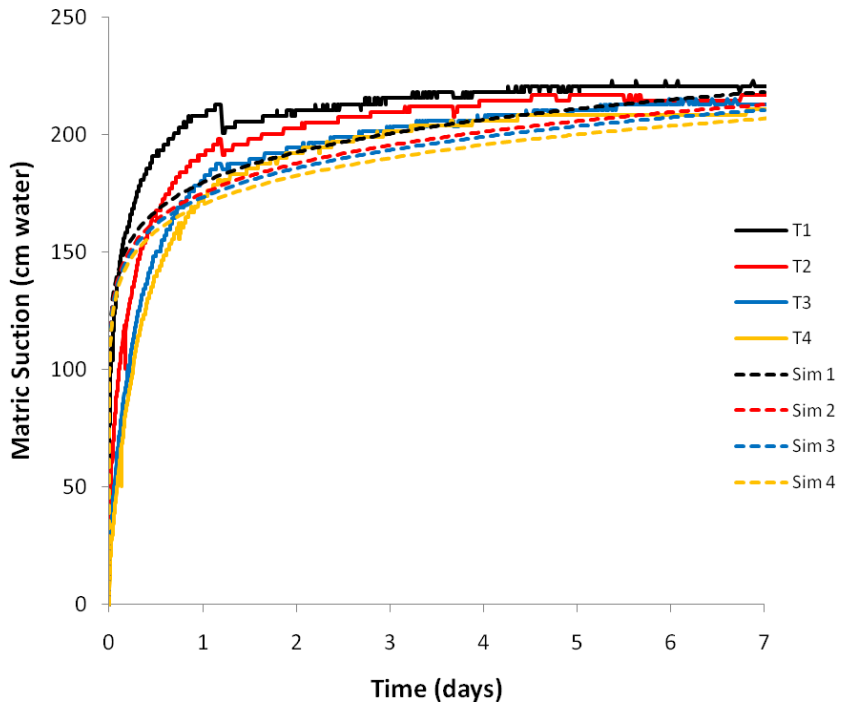

Figure 3.3. Measured and Simulated Matric Suctions (cm water) for Experiment 2

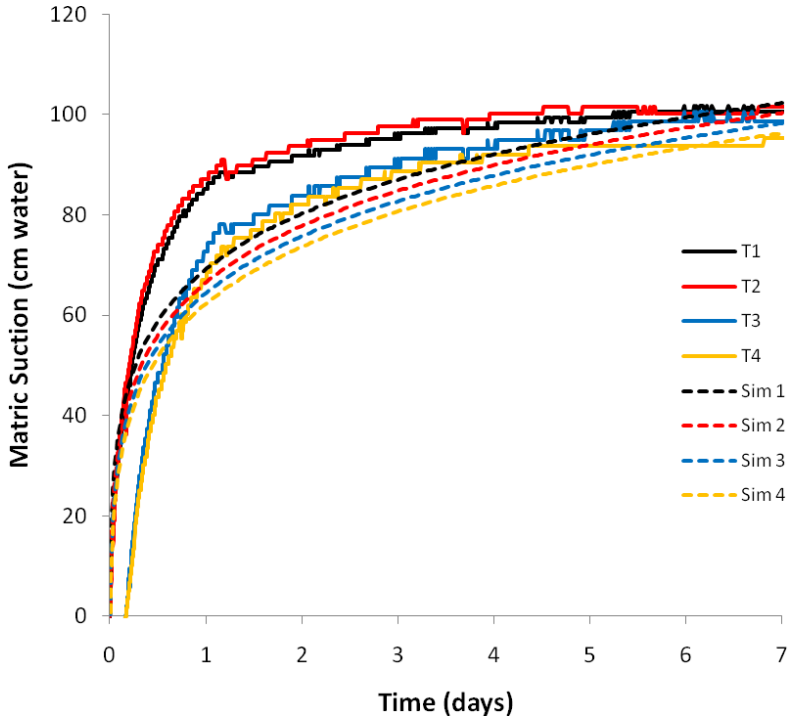

Figure 3.4. Measured and Simulated Matric Suctions (cm water) for Experiment 3

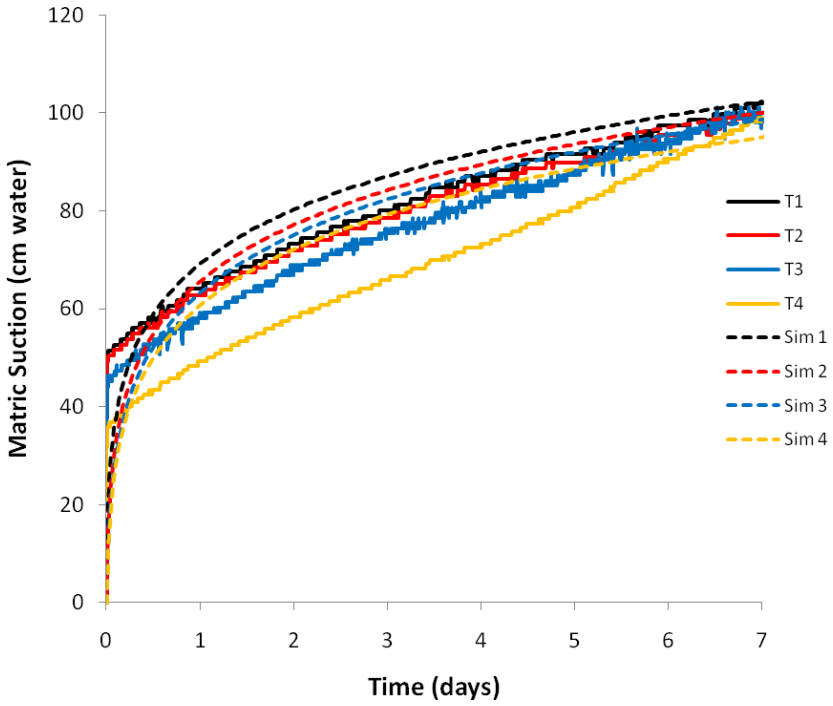

Figure 3.5. Measured and Simulated Matric Suctions (cm water) for Experiment 4

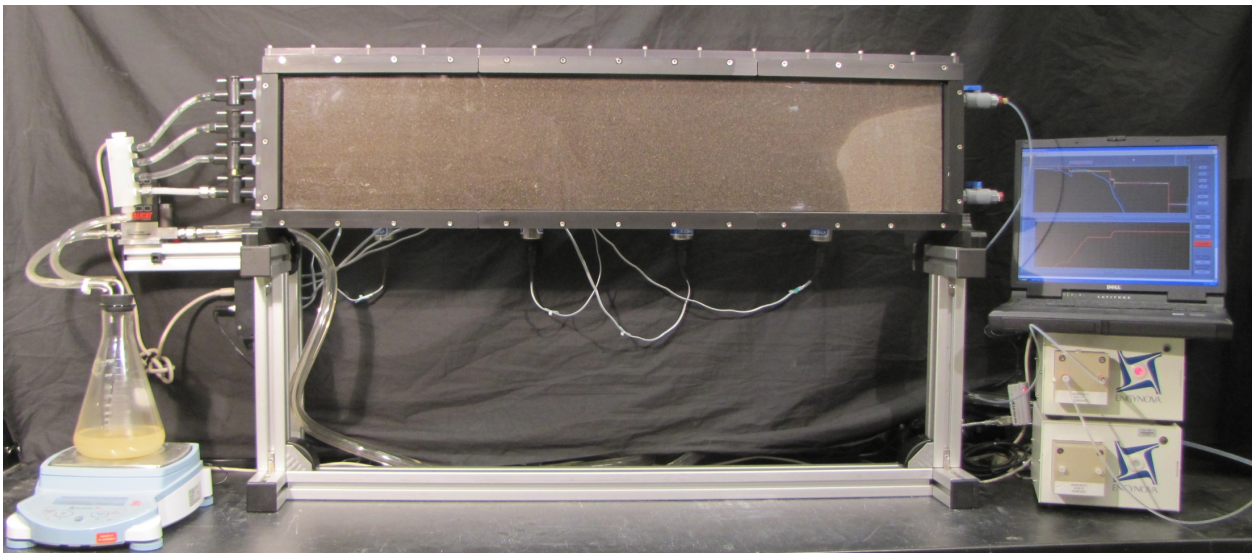

Figure 3.6. Desiccation Phenomena Observed During Continued Vacuum Application After Water Extraction Has Ceased for Experiment 1

3.2 Extraction from Experiments with Well-Pack Sand

In the field, the imposed vacuum is not directly applied to the sediment intended to be dewatered through pore-water extraction. Typically, the extracted water has to be transported through a well-pack sand before it enters the wellbore. Initial scoping tests in 1-m-long columns with different partially saturated uniform sands demonstrated that for coarser-grained sands the small relative permeability of

desaturated sands prevented any meaningful cumulative outflow over several days of imposed suction. The only configuration resulting in somewhat sustained rates was for fine-grained sands with a relatively high entry pressure. For that reason, two flow cell experiments (Experiments 5 and 6) were conducted with a fine-grained sieved 140-mesh sand. The hydraulic properties of the sand are listed in Table 2.2. The results of the two experiments with well-pack sand were largely affected by the entry pressure of the 140-sand in relationship to the imposed suction. In Experiment 5, the imposed vacuum was not enough to drain even the largest pores of the sand. As a result, no air was moved and the imposed pressure drop was largely absorbed by the low-permeability sand. Such a system with a saturated sand allows for a continued production of water, although the rate is considerably lower than for the homogeneous cases without the well-pack sand (Figure 3.5). For Experiment 6, the imposed suction was larger than the entry pressure and some limited desaturation of the sand occurred. However, the desaturation was not sufficient to stop water production even though the cumulative outflow was lower for this experiment than for Experiment 5. This result shows that if a relatively uniform wet sand is used as the well-pack material, care should be taken to not exceed the entry pressure. If the entry pressure is exceeded, rapid water desaturation occurs and the well-pack relative permeability decreases considerably. As a result, the intended pore-water extraction under these conditions will be very slow.

For Experiment 5, the gas pressures recorded by the four transducers remained atmospheric. Only slight gradients (on the order of a few cm) were observed for Experiment 6. For both of these experiments the water pressures in the sediment were considerably lower than for Experiments 1 – 4. The water pressures for Experiments 5 and 6 are shown in Figure 3.6 and Figure 3.7, respectively. These results are consistent with the lower production rate and the higher remaining saturations in the SXsim porous medium.

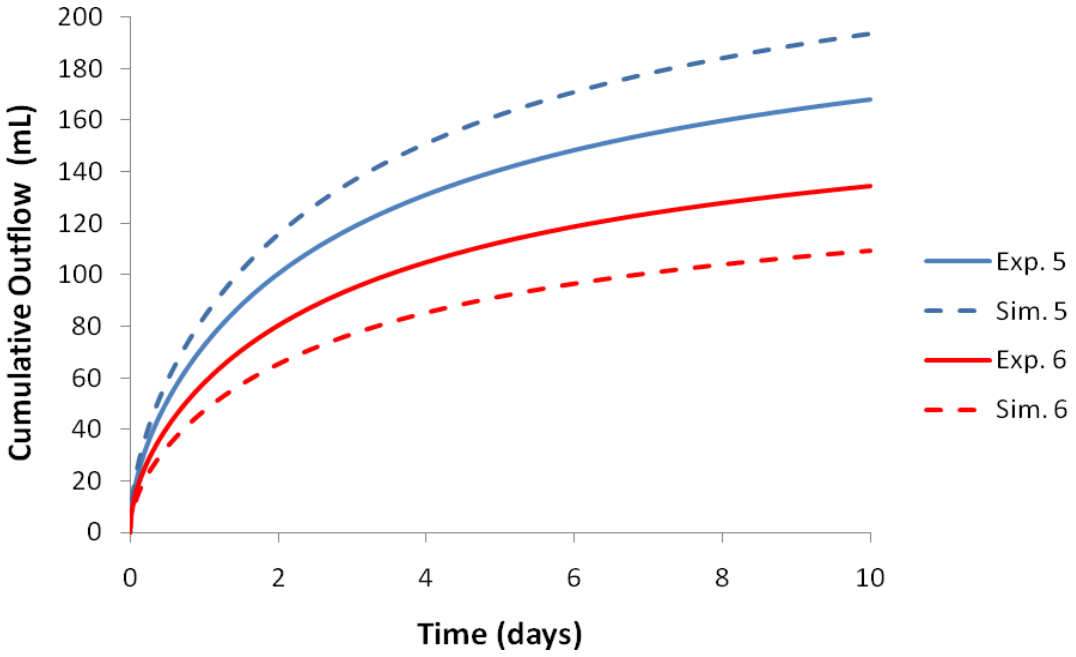

Figure 3.7. Simulated and Observed Cumulative Outflow (mL) as a Function of Time for Experiments 5 and 6

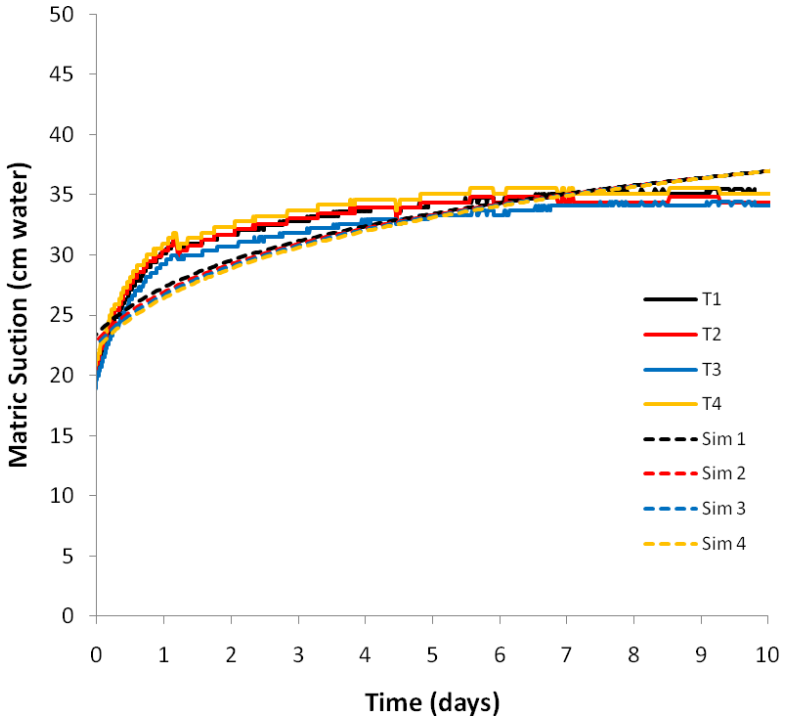

Figure 3.8. Measured and Simulated Matric Suctions (cm water) for Experiment 5

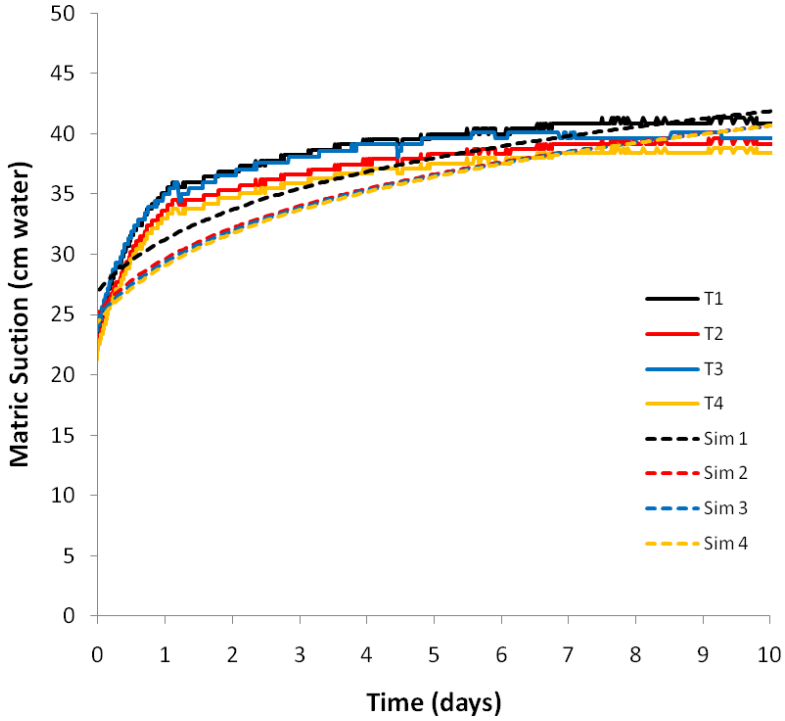

Figure 3.9. Measured and Simulated Matric Suctions (cm water) for Experiment 6

4.0 Conclusions

The flow cell experiments demonstrate that sustained pore-water extraction from unsaturated sediments can be obtained under the highly controlled conditions in the laboratory. The design was such that moving air was forced to travel through the sediment imposing pressure gradients directly on the targeted sediment so that pore water moved towards the extraction boundary of the system. Under field conditions, water cumulative outflow may be affected by preferential gas flow in relatively coarse-grained, highly permeable sediments and/or issues with well-pack sand configurations. This study was limited to relatively simple homogeneous systems to demonstrate the potential phenomena related to pore-water extraction. More complex systems with horizontal heterogeneities and more advanced well configurations were not investigated in this study.

In the experiments where a zero flux water boundary condition was imposed, the results show that application of vacuum in a controlled manner leads to a sustained but decreasing pore-water extraction rates until the water pressure gradients towards the extraction boundary approach zero. It was also observed that after water extracted had ceased, continued application of the vacuum resulted in desiccation near the boundary where gas was entering the flow cell. The incoming air, with a humidity of around 30%, was able to remove water from the porous medium in the form of water vapor as this air moved through the flow cell. Injection of air with a high humidity is not recommended because potential condensation might lead to vertical movement of water containing contaminants.

The experimental data show that increased cumulative outflow was obtained with an increase in initial water content, an increase in applied negative pressure (suction), and when the water-supplying sediment was not limited. The experimental matrix was too limited to arrive at conclusions related to maximizing water outflow rates for field conditions.

Coarse- and medium-grained well-pack sands are not recommended for pore-water extraction operations. An imposed vacuum might reduce the relative permeability of these porous media to a value too small to lead to meaningful water removal. In these experiments, an initially saturated fine-grained well-pack sand was used instead to allow for a continuous path for water removal through the sand. The inclusion of a fine-grained well-pack sand resulted in lower production rates than for the configuration without well-pack sand.

The simulated outflow data were reasonably close to the experimental observations for all experiments. This result indicates that numerical simulations could be used with some level of confidence to support the design of fields-scale applications of this method.

Future experimental work should focus on the effects of permeability contrasts on water production for layered unsaturated systems. In the field, preferential gas movement through larger permeability layers might result in insufficient water pressure gradients in the layers containing the contaminated water that is intended to be removed from the subsurface. The effects of this potentially unfavorable configuration need to be investigated in well-controlled laboratory conditions. In addition, plausible well configurations (sand type, saturations, screen materials) may need to be tested experimentally before designing a well configuration for field application.

5.0 References

Mualem Y. 1976. "A new model predicting the hydraulic conductivity." *Geoderma* 65:81-92.

Oostrom M, TW Wietsma, JH Dane, MJ Truex, and AL Ward. 2009. "Desiccation of unsaturated porous media: Intermediate-scale experiments and numerical simulation." *Vadose Zone J*. 8:643-650.

Schroth MH, SJ Ahearn, JS Selker, and JD Istok. 1996. "Characterization of miller-similar silica sands for laboratory hydrologic studies." *Soil Sci. Am. J*., 60:1331-1339.

Serne RJ, RE Clayton, IV Kutnyakov, HT Schaef, VL LeGore, DS Burke, BN Bjornstad, RD Orr, TC Wilson, DC Lanigan, MJ O'Hara, BA Williams, GW Gee, CF Brown, CW Lindemeier, and GV Last. 2002a. *Characterization of Vadose Zone Sediment: Borehole 299-W23-19 [SX-115] in the S-SX Waste Management Area.* PNNL-13757-2, Pacific Northwest National Laboratory, Richland, Washington.

Serne RJ, RE Clayton, IV Kutnyakov, GV Last, VL LeGore, TC Wilson, HT Schaef, MJ O'Hara, KB Wagnon, DC Lanigan, CF Brown, BA Williams, CW Lindenmeier, RD Orr, DS Burke, and CC Ainsworth. 2002b. *Characterization of Vadose Zone Sediment: Borehole 41-09-39 in the S-SX Waste Management Area.* PNNL-13757-3, Pacific Northwest National Laboratory, Richland, Washington.

Serne RJ, RE Clayton, IV Kutnyakov, GV Last, VL LeGore, TC Wilson, HT Schaef, MJ O'Hara, KB Wagnon, DC Lanigan, CF Brown, BA Williams, CW Lindenmeier, RD Orr, DS Burke, and CC Ainsworth. 2002c. *Characterization of Vadose Zone Sediment: Slant Borehole SX-108 in the S-SX Waste Management Area.* PNNL-13757-4, Pacific Northwest National Laboratory, Richland, Washington.

U.S. Deprtment of energy (DOE). 2010. *Characterization of the Soil Desiccation Pilot Test Site*. DOE/RL-2009- 119, U.S. Department of Energy, Richland Operations Office, Richland, Washington.

van Genuchten MTh. 1980. "A closed-form equation for predicting the hydraulic conductivity of unsaturated soils." *Soil. Sci. Soc. Am. J*. 44:892-898.

White MD and M Oostrom. 2006. *STOMP Subsurface Transport Over Multiple Phases, Version 4.0, User's Guide*. PNNL-15782, Pacific Northwest National Laboratory, Richland, Washington.

Wietsma TW, M Oostrom, MA Covert, TW Queen, and MJ Fayer. 2009. "An automated apparatus for constant flux, constant head, and falling head hydraulic conductivity measurements." *Soil Science Society of America J*. 73: 466-470.

Appendix A

Example Numerical Simulation Input File, Experiment 1

Appendix A - Example Numerical Simulation Input File, Experiment 1

```
~Simulation Title Card
1,
Simulation of Pore Water Extraction Experiment 1,
Mart Oostrom,
PNNL,
April 2011,
,
2,
Experiment 1 (Base Case),
100 cm suction,

~Solution Control Card
Normal,
Water-Air-Energy,
1,
0.0,d,10,d,0.01,s,1,d,1.25,8,1.e-06,
1,
Variable Aqueous Diffusion,
Variable Gas Diffusion,
0,

~Grid Card
Cartesian,
100,1,20,
0,cm,100@1.0,cm,
0,cm,1@5.0,cm,
0,cm,20@1.0,cm,

~Inactive Nodes Card
0,

~Rock/Soil Zonation Card
1,
Hanford Mixture,1,100,1,1,1,20,

~Mechanical Properties Card
Hanford Mixture,2650,kg/m^3,0.34,0.34,,,,

~Hydraulic Properties Card
Hanford Mixture,1.23,hc:m/d,1.23,hc:m/d,1.23,hc:m/d,

~Saturation Function Card
Hanford Mixture,Van Genuchten,0.061,1/cm,3.24,0.16,,

~Thermal Properties Card
```

```
Hanford Mixture,Constant,2.0,W/m K,2.0,W/m K,2.0,W/m K,781,J/kg K,

~Aqueous Relative Permeability Card
Hanford Mixture,Mualem,,

~Gas Relative Permeability Card
Hanford Mixture,Mualem,,

~Initial Conditions Card
Aqueous Pressure,Gas Pressure,
3,
#
# Initially implied suction of 18 cm to establish initial
# conditions
#
Aqueous Pressure, 99535,Pa,,,,,-9793.517,1/m,1,100,1,1,1,20,
Gas Pressure,101325,Pa,,,,,-11.71,1/m,1,100,1,1,1,20,
Temperature,20,C,,,,,,,1,100,1,1,1,20,

~Boundary Conditions Card
2,
West,Outflow Energy,Dirichlet-outflow,Dirichlet,
1,1,1,1,1,20,1,
#
# 100 cm suction is imposed on west side of flow cell
#
0,d,,,91531.483,Pa,1.0,91531.483,Pa,1.0,
East,Dirichlet,Zero Flux,hydraulic gradient,
100,100,1,1,1,20,1,
0,hr,20,C,,Pa,1.0,101325,Pa,1.0,

~Output Control Card
4,
#
# monitoring ports at 4 locations
#
13,1,10,
38,1,10,
63,1,10,
88,1,10,
1,1,d,cm,6,6,6,
7,
integrated water mass,kg,
aqueous saturation,,
aqueous pressure,pa,
matric potential,cm,
gas pressure,Pa,
xnc aqueous vol[umetric flux (node centered)],cm/day,
znc aqueous vol[umetric flux (node centered)],cm/day,
0,
9,
```

aqueous saturation,,
aqueous pressure,pa,
matric potential,,
temperature,C,
gas saturation,,
gas pressure,Pa,
xnc gas volumetric flux,cm/day,
znc gas volumetric flux,cm/day,
no restart,,

~Surface Flux Card
4,
Aqueous Volumetric Flux,mL/day,mL,West,1,1,1,1,1,20,
Aqueous Volumetric Flux,mL/day,mL,East,100,100,1,1,1,20,
Gas Volumetric Flux,mL/day,mL,West,1,1,1,1,1,20,
Gas Volumetric Flux,mL/day,mL,East,100,100,1,1,1,20,

Distribution

No. of Copies		
2	DOE Office of River Protection	
	RW Lober	PDF
3	Washington River Protection Solutions	
	MB Skorska	PDF
	DA Myers	PDF
	SJ Eberlein	PDF

No. of Copies		
5	**Local Distribution**	
	Pacific Northwest National Laboratory	
	VL Freedman	PDF
	M Oostrom	PDF
	MJ Truex	PDF
	MD White	PDF
	Hanford Technical Library	PDF

Pacific Northwest
NATIONAL LABORATORY

U.S. DEPARTMENT OF
ENERGY

902 Battelle Boulevard
P.O. Box 999
Richland, WA 99352
1-888-375-PNNL (7665)
www.pnl.gov